Electronic Supplementary Information (ESI)

Transforming Molecular Orientation of Crystalline Lamellae by the Degree of Multi-Fluorination within D-A Copolymers and its Effect on Photovoltaic Performance

Jianhong Gao[a], *Wei Wang*[a], *Yanqi Hu*[a], *Chun Zhan*[a], *Shengqiang Xiao*[*a], *Xinhui Lu*[*b], *and Wei You*[* ac]

[a] State Key Laboratory of Advanced Technology for Materials Synthesis and Processing Wuhan University of Technology, Wuhan, 430070, P. R. China. E-mail: *E-mail:shengqiang@whut.edu.cn

[b] Department of Physics, Chinese University of Hong Kong, Hong Kong, P. R. China. *E-mail: xhlu@phy.cuhk.edu.hk

[c] Department of Chemistry, University of North Carolina at Chapel Hill, Chapel Hill, North Carolina 27599-3290, United States. *E-mail: wyou@unc.edu

The list of the content:

1. Materials
2. Measurements and instruments.
3. Fabrication and characterization of polymer solar cells.
4. ^{1}H, ^{13}C-NMR and high resolution MALDI-TOF mass spectrometry of the compounds in this work (**Fig. S1**- **Fig. S17**)
5. Supplementary figures and tables:

   a) TGA curves of the two copolymers at a heating rate of 10 ^{o}C min^{-1} under nitrogen (**Fig. S18**).

   b) Cyclic voltammogram curves of the two copolymers in thin film (**Fig. S19**).

   c) *J-V* characteristics of polymers:PC$_{71}$BM PSCs in conventional architecture at different D:A weight ratio (**Fig. S20**).

   d) Photovoltaic properties of Polymers:PC$_{71}$BM PSCs in conventional architecture at different D/A weight ratios (**Table S1**).

   e) The optimized photovoltaic properties of PDTBBT-3F:PC$_{71}$BM = 1:2.5 and PDTBBT-4F:PC$_{71}$BM = 1:2 PSCs in conventional architecture with processing additives of DIO and DPE (**Table S2**).

   f) Extinction coefficient spectra of BHJ blend films for optimum device based on the Polymers: PC$_{71}$BM prepared from *o*-DCB (**Fig. S21**).

   g) $J^{0.5}$ *vs* V_{appl}-V_{bi}-V_{rs} plots for hole-only and electron-only devices of PDTBBT-3F and PDTBBT-4F blend films (**Fig. S22**)

   h) Tapping-mode AFM height and phase images of the optimized BHJ blends (**Fig. S23**).

   i) Physical parameters of PDTBBT-3F:PC$_{71}$BM and PDTBBT-4F:PC$_{71}$BM devices (**Table S3**).

   j) The coherence length (L_C) and full width at half-maximum (FWHM) along both OOP and IP direction of the neat PDTBBT-3F and PDTBBT-4F, and the corresponding polymer:PC$_{71}$BM blend films (**Table S4**).

1. Materials

4,7-dibromo-5,6-difluorobenzo[c][1,2,5]thiadiazole and 4,7-dibromo-5-fluorobenzo[c][1,2,5]-thiadiazole were purchased from Derthon. [6,6]-Phenyl C_{71}–butyric acid methyl ester ($PC_{71}BM$) was purchased from Solenne. Other reagents were used as purchased from JK Chemical and Energy Chemical. Anhydrous THF was obtained by distillation over sodium/benzophenone under nitrogen atmosphere.

2. Measurements and Instruments

^1H and ^{13}C NMR spectrum were recorded on a Bruker AV500 at 500 MHz using deuterated chloroform ($CDCl_3$) as the solvent. The molecular weights of two polymers were determined by high temperature gel-permeation chromatography (GPC) with trichlorobenzne as the eluent at 150 ℃ relative to a polystyrene standard on an Agilent PL-GPC 220 system. Thermogravimetric analysis measurements were carried out on NETZSCH (STA449F3) at a heating rate of 10 °C min^{-1} under nitrogen. Room temperature UV−vis spectra of polymer solutions and films were recorded on a SHIMADZU UV-1750 spectrophotometer. The dilute solutions were prepared as followings: we first prepared the polymer solutions with a concentration of 10 mg mL^{-1} in dichlorobenzene, and then took 40 μL of them with a micro syringe and injected into appropriate amount of dichlorobenzene (volume with dichlorobenzene to 4 mL) to attain a concentration of 1×10^{-5} mg mL^{-1}. Solution UV-Vis absorption spectra at elevated temperatures were collected on Perkin Elmer Lambda 750 UV/VIS/NIR Spectrometer. The temperature-dependent experiments were measured through stepwise increasing temperature from room temperature to fully disaggregate temperature (such as 100 ℃). Cyclicvoltammetry (CV) experiments were performed with CHI 660D analyzer. All CV measurements were carried out in 0.1 M tetrabutylammonium hexafluorophosphate (Bu_4NPF_6) in anhydrous acetonitrile with a conventional three-electrode configuration employing a platinum wire as a counter electrode, platinum electrode coated with a thin polymer film as a working electrode, and Ag/Ag^+ electrode as a reference electrode at a scan rate of 80 mV s^{-1}. The atomic force microscopy (AFM) images (5.0 μm × 5.0 μm) were obtained through tapping mode on Multimode 8 SPM at ambient condition. RTESPA (0.01 - 0.025 ohm-cm Antimony (n) doped silicon) tips with a spring constant of 20 - 80 N m^{-1} and a frequency of 305 - 356 kHz were used in

imaging. The GIWAXS measurements of the pristine polymers and polymer:fullerene blend films were conducted at 23 A SWAXS beamline of a superconductor wiggler at the National Synchrotron Radiation Research Center, Hsinchu, Taiwan, using 10 keV beam incident at 0.15° and a C9728DK area detector.

3. Fabrication and Characterization of Polymer Solar Cells

The PSC devices were fabricated with the conventional configuration of ITO/PEDOT:PSS/donor (PDTBBT-3F or PDTBBT-4F):$PC_{71}BM$ /Ca (~ 20 nm)/Al (80 nm). Prior to be used, indium tin oxide glass substrates were sequentially cleaned with distilled water, acetone, iso-propanol and were treated by UV-Ozone. For BHJ devices, poly(3,4-thylenedioxythiophene):polystyrenesulfonic acid (PEDOT:PSS) was spin-coated onto the ITO substrate and annealed at 150 °C for 20 min. To prepare the BHJ films, the polymers of PDTBBT-3F or PDTBBT-4F (10 mg mL^{-1}) were blended with $PC_{71}BM$ in o-dichlorobenzene (o-DCB), respectively. BHJ films were spin-cast on the top of the PEDOT:PSS layers in a N_2 filled glove box. Subsequently, Ca (20 nm) and Al (80 nm) were sequentially deposited on the top of the active layers as the cathode at a pressure of 2×10^{-6} mbar through a shadow mask that defines 8 devices with each active area of 0.09 cm^2.

Current-voltage measurements were carried out in a glovebox under AM 1.5 G irradiation (100 mW cm^{-2}) from a 450 W solar simulator (Newport 94023A-U) calibrated by a NREL certified standard silicon cell. Current versus potential (J-V) curves were recorded with a Keithley 2420 digital source meter. For external quantum efficiency (EQE) tests, the devices were transferred by a self-made testing box from the glovebox into the chamber of a 7-SCSpec spectral performance of solar cell test system consisting of a 500 watt SCS028-7ILX500 xenon light source, a 7ISW301 vertical grating spectrometer, a 71FW6 filter wheel, a SR810 lock-in amplifier. The calibration of the incident monochromatic light was carried out with a Hamamatsu S1337-1010 BQ Silicon photodetector.

The SCLC J-V curves were obtained in the dark from the electron-only and hole-only devices of ITO/ZnO/active-layer/Ca/Al and ITO/PEDOT:PSS/active-layer/MoO$_3$/Ag, respectively. The electron and hole mobility were calculated using the Mott-Gurney square law, $J = (9/8)\varepsilon_0\varepsilon_r\mu(V^2/L^3)$, where ε_0 is vacuum permittivity, ε_r is the dielectric constant of the polymer used, μ is the charge

carrier mobility, V is the effective applied voltage, and L is the thickness of the active film in the device.

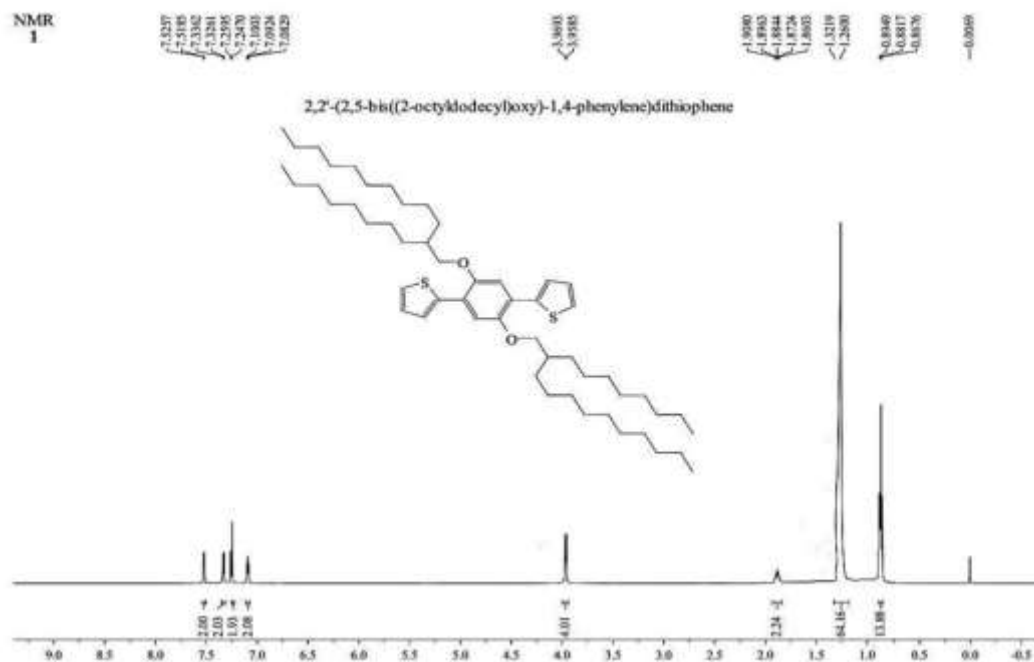## 4. ¹H, ¹³C-NMR and high resolution MALDI-TOF mass spectrometry of new compounds in this work

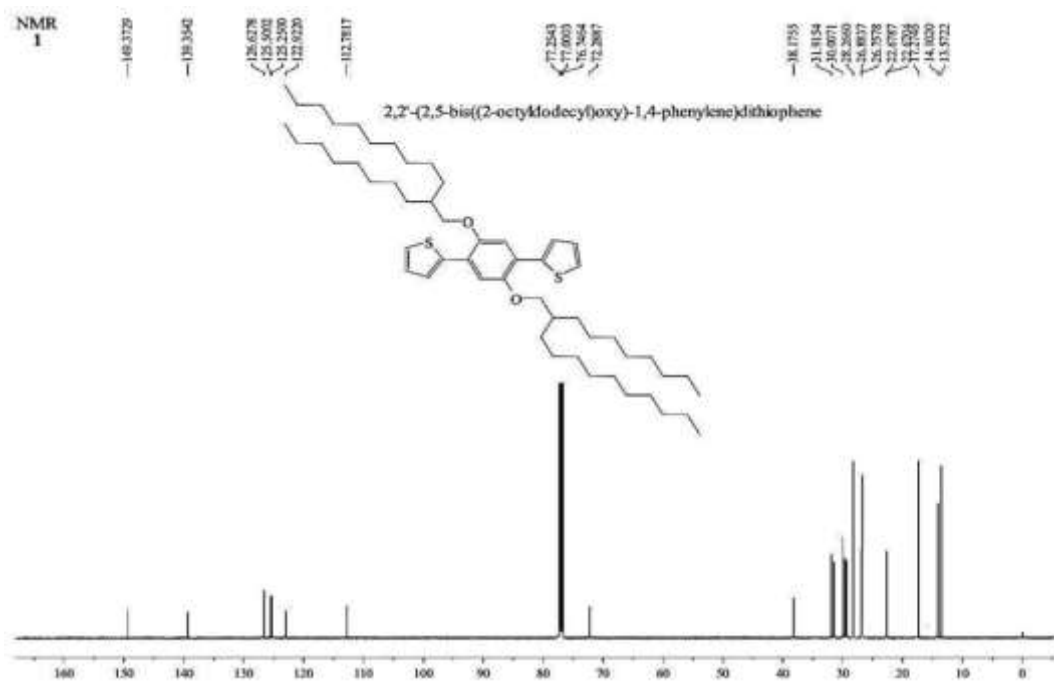**Fig. S1** ¹H NMR of 2,2'-(2,5-bis((2-octyldodecyl)oxy)-1,4-phenylene)dithiophene (1).

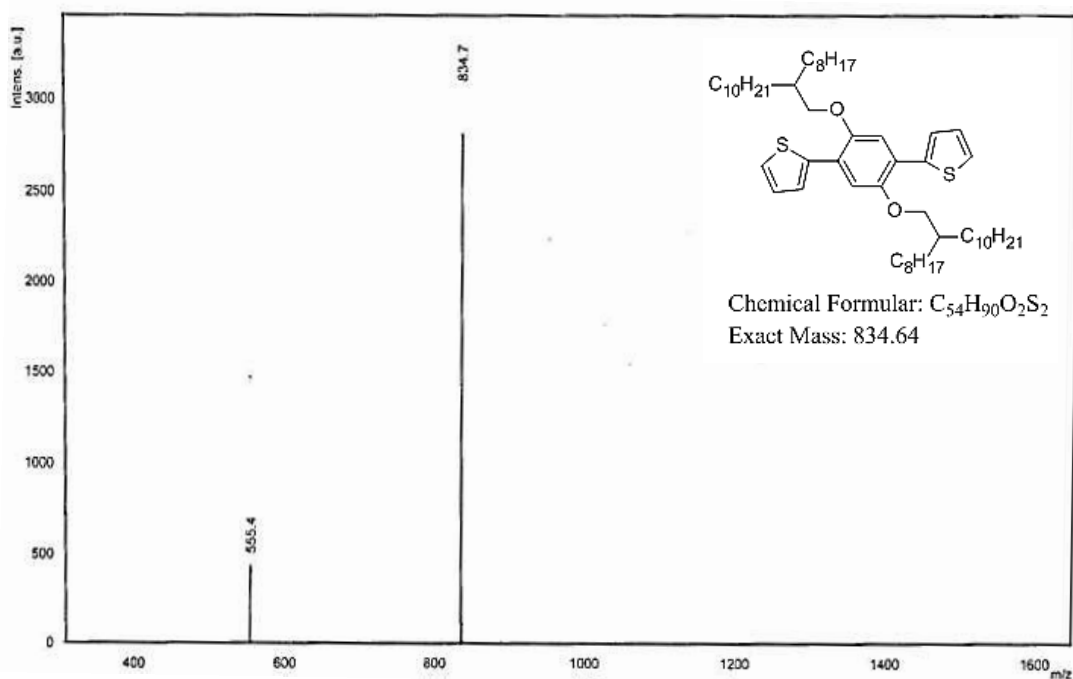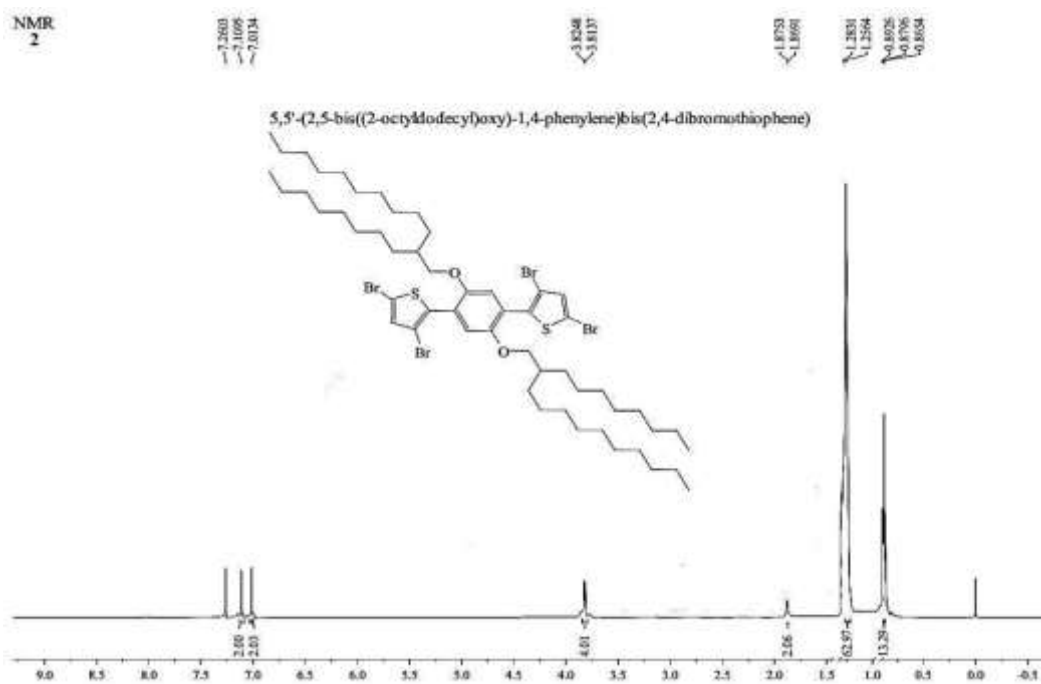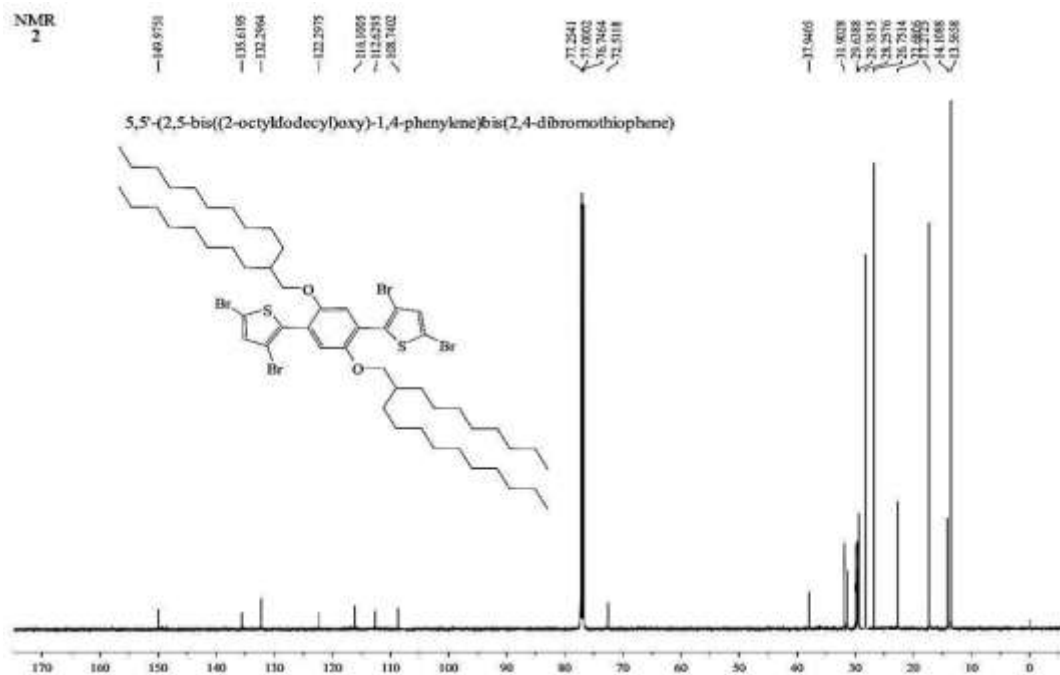**Fig. S2** ¹³C NMR of 2,2'-(2,5-bis((2-octyldodecyl)oxy)-1,4-phenylene)dithiophene (1).

Fig. S3 MALDI-TOF mass spectrometry of
2,2'-(2,5-bis((2-octyldodecyl)oxy)-1,4-phenylene)dithiophene (1).

Fig. S4 ^{1}H NMR of 5,5'-(2,5-bis((2-octyldodecyl)oxy)-1,4-phenylene) bis(2,4-dibromothiophene) (2).

Fig. S5 ^{13}C NMR of 5,5'-(2,5-bis((2-octyldodecyl)oxy)-1,4-phenylene) bis(2,4-dibromothiophene) (2).
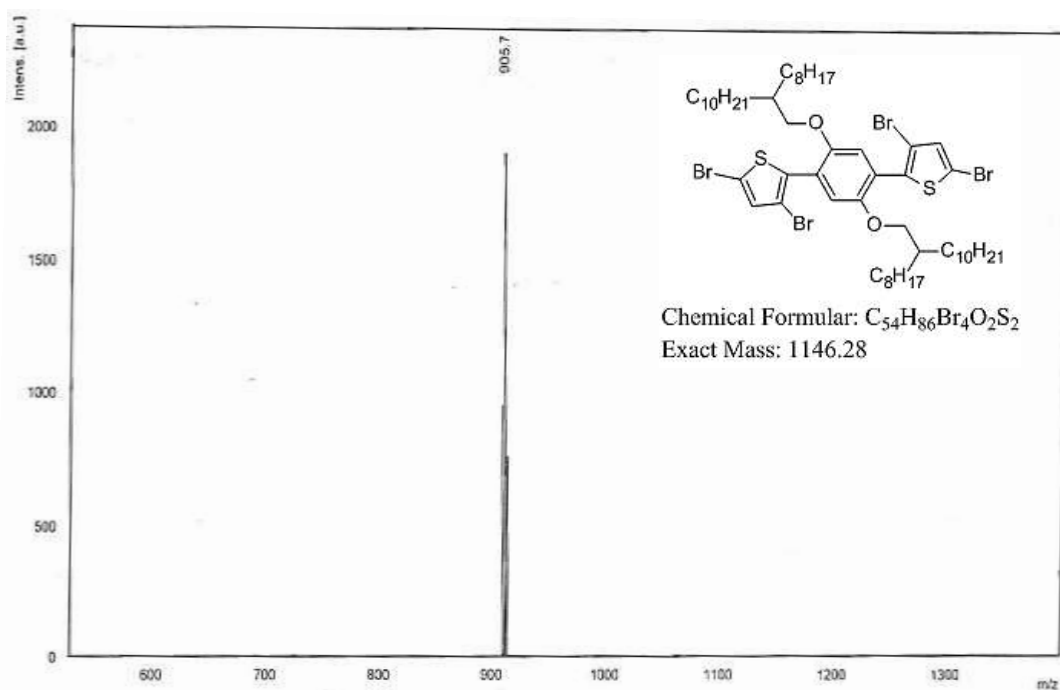

Fig. S6 MALDI-TOF mass spectrometry of 5,5'-(2,5-bis((2-octyldodecyl)oxy)-1,4-phenylene) bis-(2,4-dibromothiophene) (2).
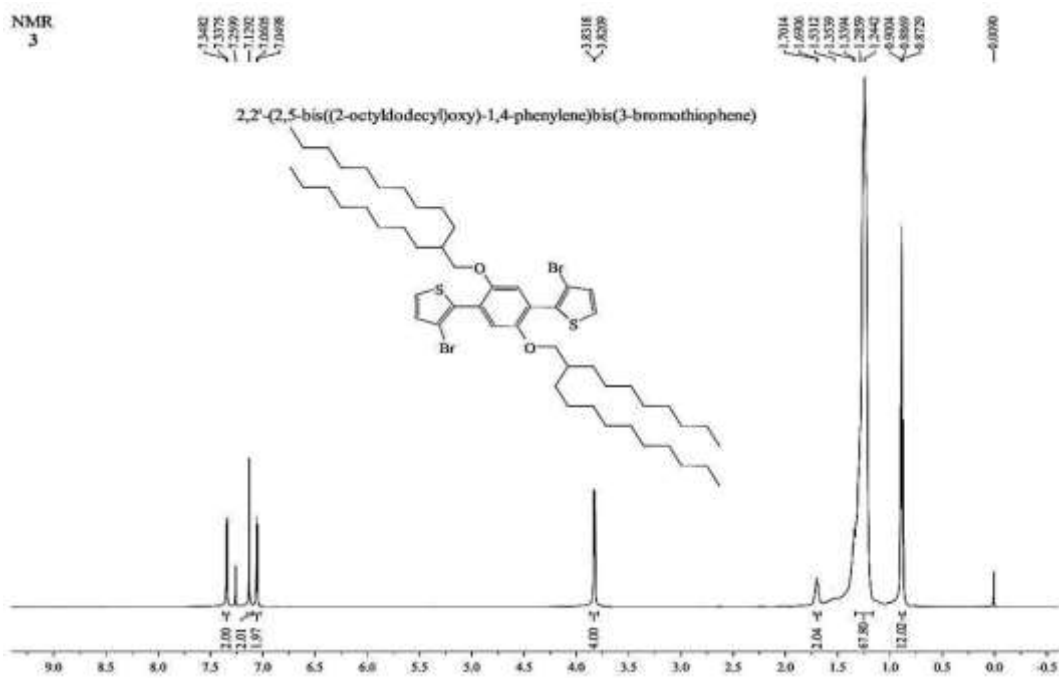
Fig. S7 ^{1}H NMR of 2,2'-(2,5-bis((2-octyldodecyl)oxy)-1,4-phenylene)bis(3-bromothiophene) (3).
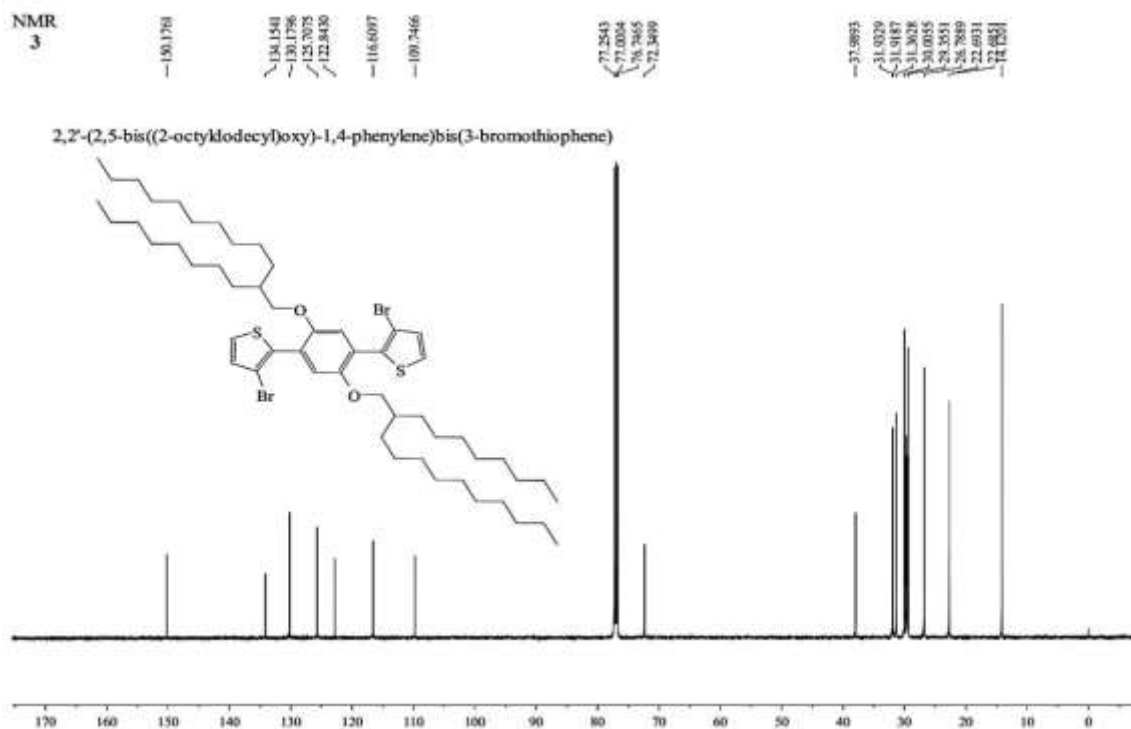

Fig. S8 ^{13}C NMR of 2,2'-(2,5-bis((2-octyldodecyl)oxy)-1,4-phenylene) bis(3-bromothiophene) (3).
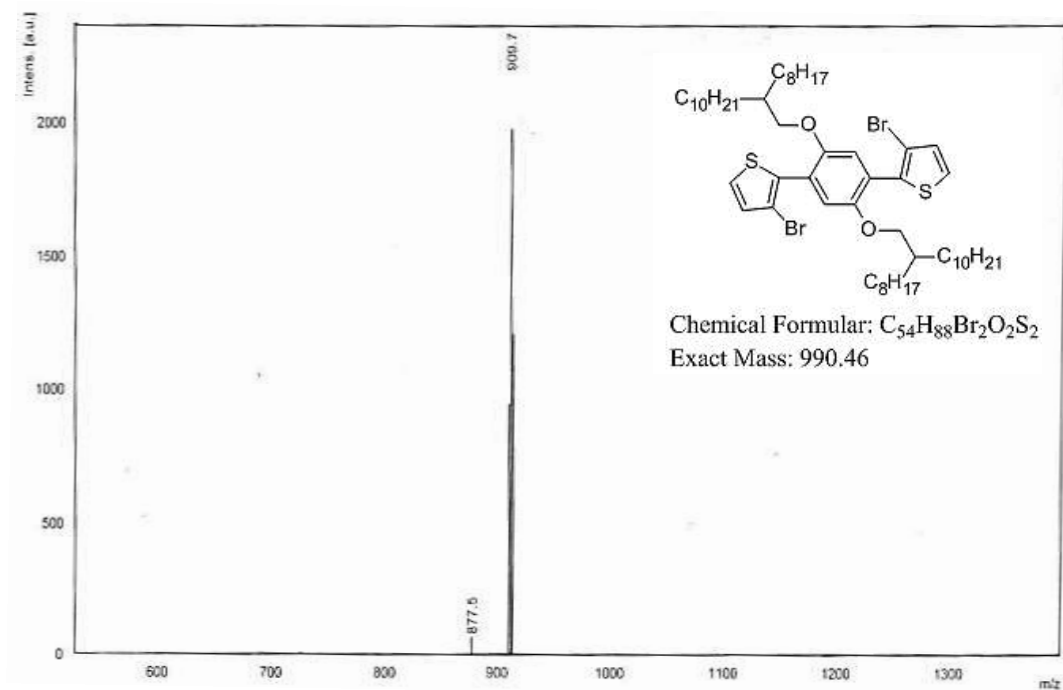
Fig. S9 MALDI-TOF mass spectrometry of 2,2'-(2,5-bis((2-octyldodecyl)oxy)-1,4-phenylene)bis-(3-bromothiophene) (3).
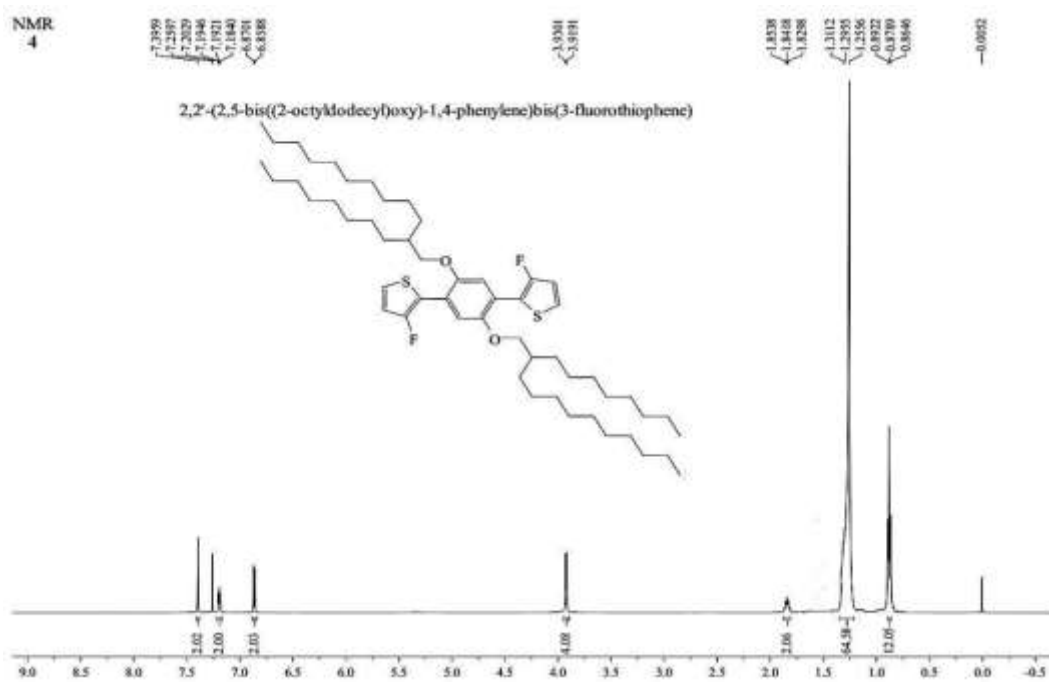

Fig. S10 ^{1}H NMR of 2,2'-(2,5-bis((2-octyldodecyl)oxy)-1,4-phenylene)bis(3-fluorothiophene) (4).
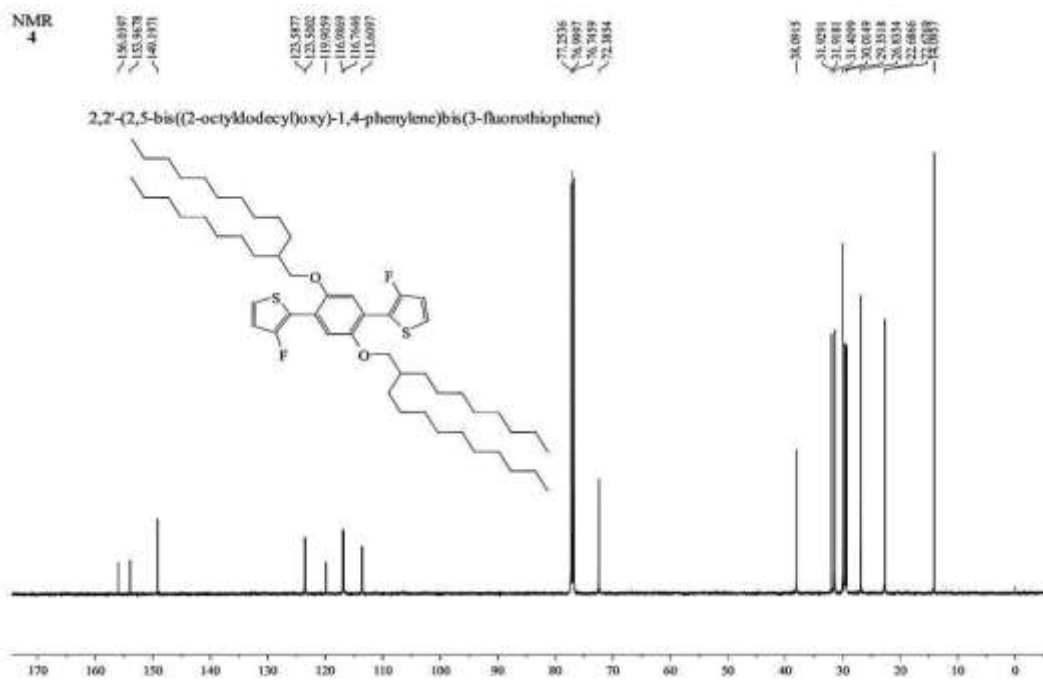
Fig. S11 ^{13}C NMR of 2,2'-(2,5-bis((2-octyldodecyl)oxy)-1,4-phenylene)bis(3-fluorothiophene) (4).
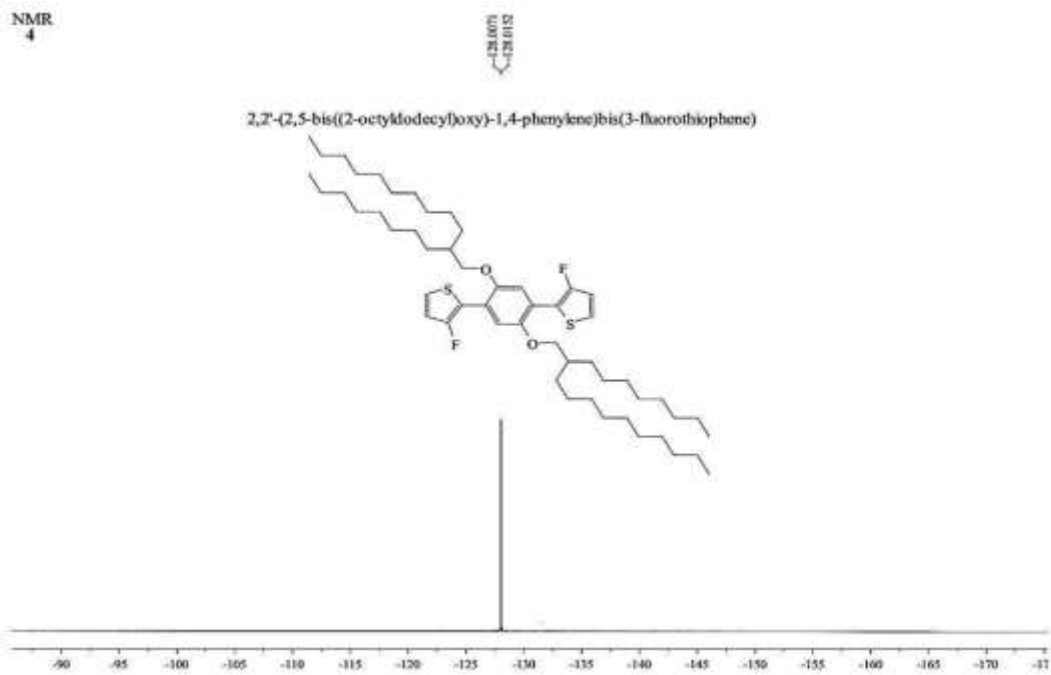

Fig. S12 ^{19}F NMR of 2,2'-(2,5-bis((2-octyldodecyl)oxy)-1,4-phenylene)bis(3-fluorothiophene) (4).

Fig. S13 MALDI-TOF mass spectrometry of 2,2'-(2,5-bis((2-octyldodecyl)oxy)-1,4-phenylene)bis-(3-fluorothiophene) (4).

Fig. S14 ^{1}H NMR of (5,5'-(2,5-bis((2-octyldodecyl)oxy)-1,4-phenylene)bis-(4-fluorothiophene-5,2-diyl))bis(trimethylstannane) (5).
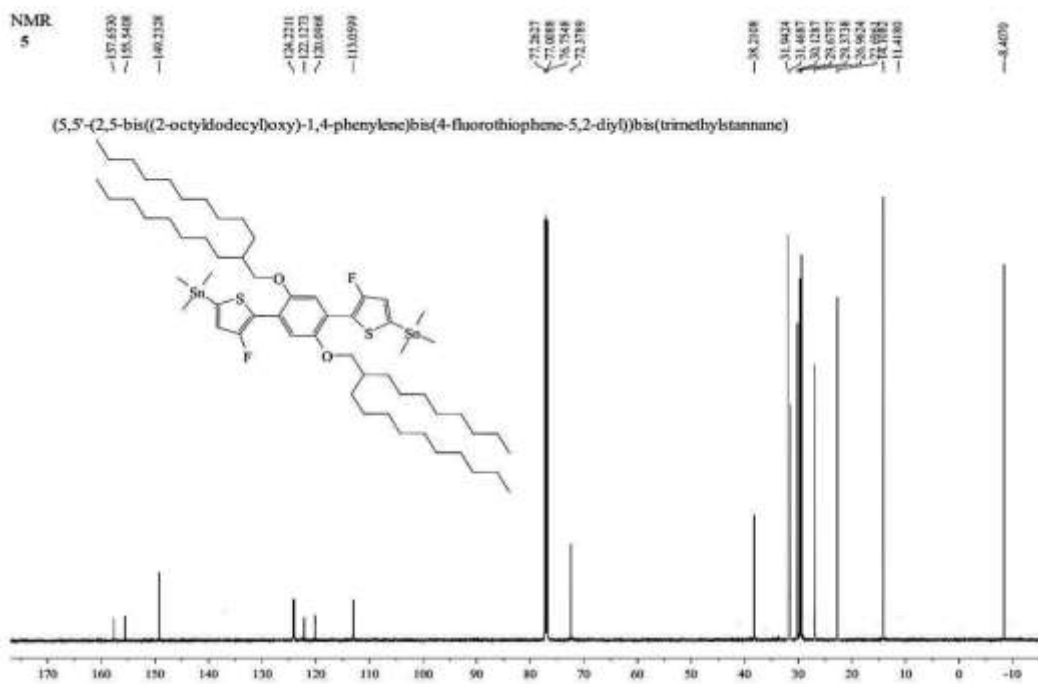
Fig. S15 ^{13}C NMR of (5,5'-(2,5-bis((2-octyldodecyl)oxy)-1,4-phenylene)bis-(4-fluorothiophene-5,2-diyl))bis(trimethylstannane) (5).
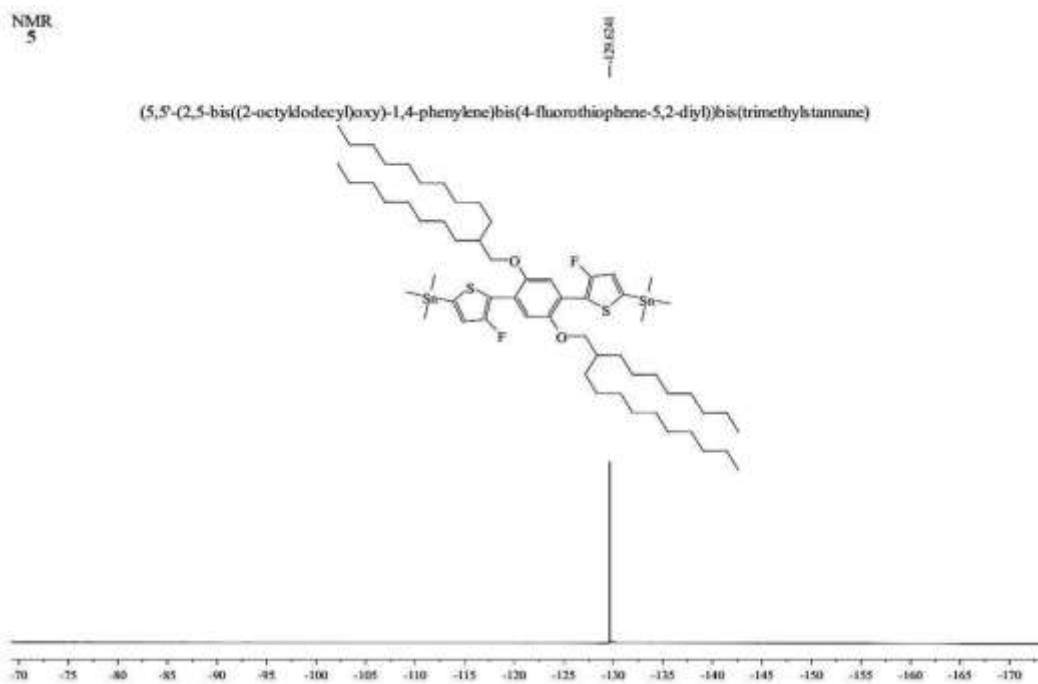

Fig. S16 ^{19}F NMR of (5,5'-(2,5-bis((2-octyldodecyl)oxy)-1,4-phenylene)bis-(4-fluorothiophene-5,2-diyl))bis(trimethylstannane) (5).
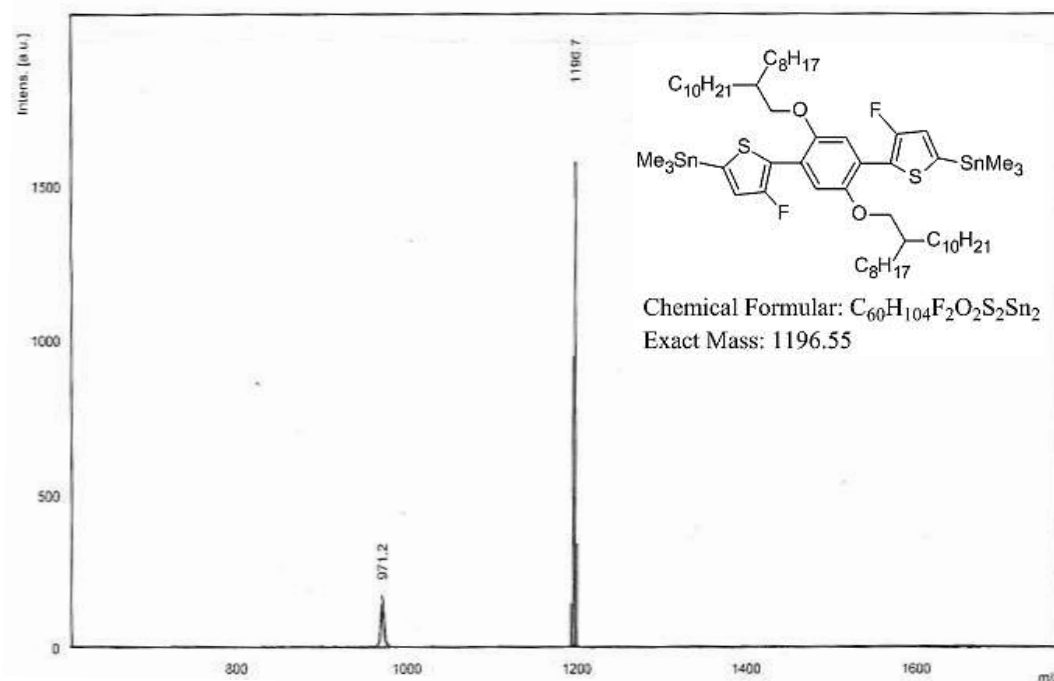
Fig. S17 MALDI-TOF mass spectrometry of (5,5'-(2,5-bis((2-octyldodecyl)oxy)-1,4-phenylene)bis-(4-fluorothiophene-5,2-diyl))bis(trimethylstannane) (5).
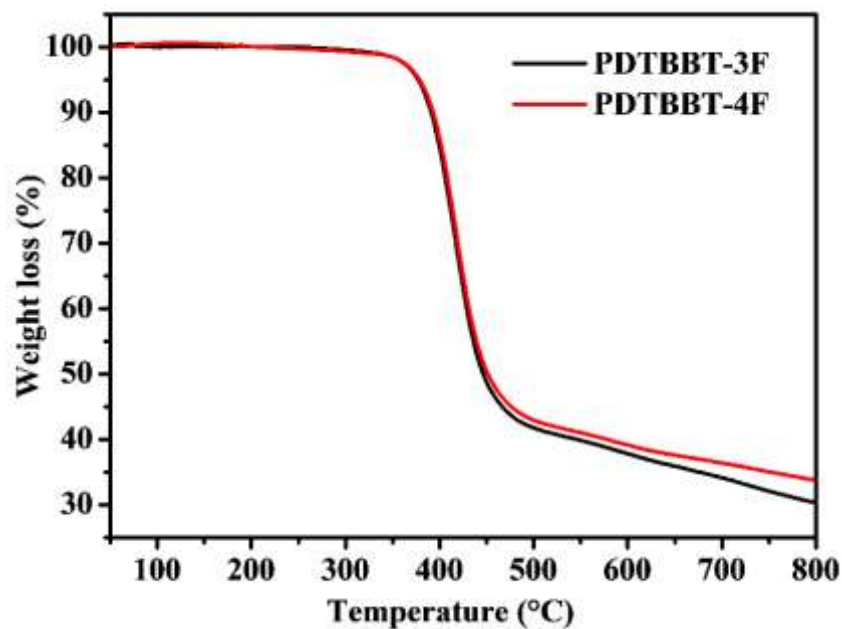
5. Supplementary Figures and Tables

Fig. S18. TGA curves of **PDTBBT-3F** and **PDTBBT-4F** at heating rate of 10 °C min^{-1} under N$_2$.
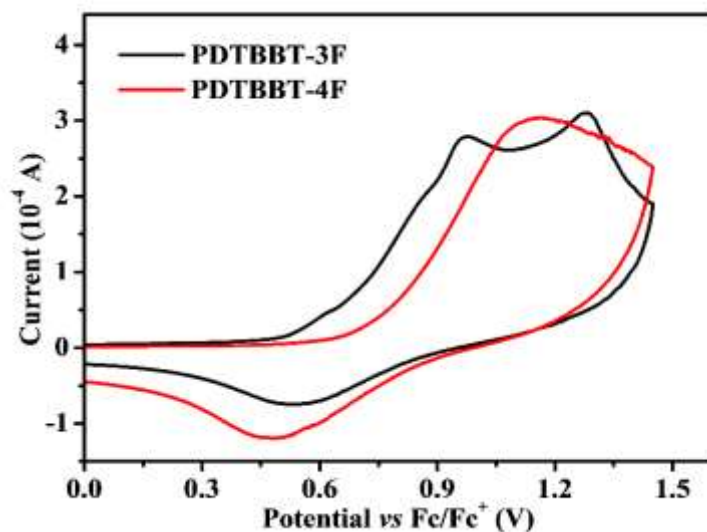
Fig. 19 Cyclic voltammograms of the polymers in thin film (drop cast from 3 mg mL^{-1} chloroform solution) measured in acetonitrile (0.1 M Bu$_4$NPF$_6$) at a scan rate of 80 mV s^{-1}.
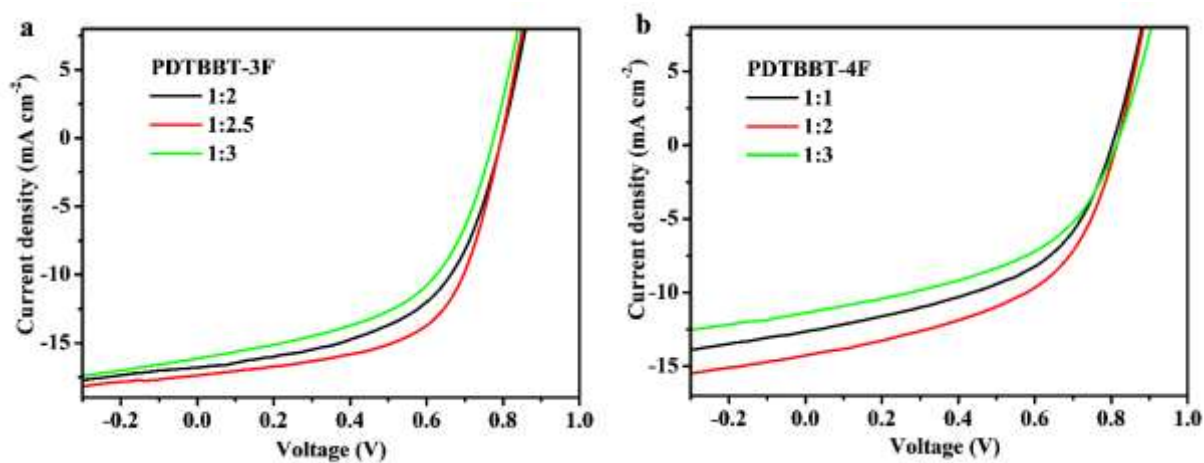

Fig. S20 *J-V* characteristics of a) **PDTBBT-3F** and b) **PDTBBT-4F** based PSCs with different polymers:PC$_{71}$BM blend ratios (solvent: *o*-DCB).

Table S1. Photovoltaic properties of Polymers:PC$_{71}$BM PSCs in conventional architecture at different D/A weight ratios ((parenthesized with the average values and standard deviations over 15 devices)

Polymer	D:A ratio (w/w)	Thickness (nm)	V_{oc} (V)	J_{sc} (mA cm^{-2})	FF (%)	PCE (%)
PDTBBT-3F	1:2	201 ± 2	0.801 (0.796 ± 0.008)	16.80 (16.52 ± 0.32)	55.3 (54.8 ± 1.0)	7.39 (7.16 ± 0.25)
	1:2.5	205 ± 3	0.804 (0.798 ± 0.009)	17.35 (17.12 ± 0.30)	59.8 (59.4 ± 0.9)	8.33 (8.15 ± 0.21)
	1:3	203 ± 3	0.768 (0.763 ± 0.007)	16.12 (15.89 ± 0.26)	52.8 (52.4 ± 0.8)	6.58 (6.41 ± 0.19)
PDTBBT-4F	1:1	178 ± 2	0.803 (0.798 ± 0.008)	12.64 (12.42 ± 0.28)	48.6 (48.1 ± 0.8)	4.95 (4.79 ± 0.23)
	1:2	185 ± 2	0.817 (0.812 ± 0.007)	14.25 (14.03 ± 0.24)	50.7 (50.3 ± 1.0)	5.92 (5.79 ± 0.16)
	1:3	190 ± 3	0.812 (0.806 ±0.01)	11.36 (11.12 ± 0.30)	47.3 (46.8 ± 0.9)	4.33 (4.18 ± 0.20)

Table S2 The optimized photovoltaic properties of PDTBBT-3F:PC$_{71}$BM = 1:2.5 and PDTBBT-4F:PC$_{71}$BM = 1:2 PSCs in conventional architecture with processing additives of DIO and DPE (v/v, o-DCB).

BHJ	Additive	V_{oc} (V)	J_{sc} (mA cm^{-2})	FF (%)	PCE [a] (%)
PDTBBT-3F:PC$_{71}$BM = 1:2.5	W/O	0.804 (0.798 ± 0.009)	17.35 (17.12 ± 0.30)	59.8 (59.4 ± 0.9)	8.33 (8.15 ± 0.21)
	1% DIO	0.785 (0.779 ± 0.008)	15.02 (14.81 ± 0.25)	49.8 (49.3 ± 0.9)	5.87 (5.73 ± 0.19)
	2% DIO	0.793 (0.786 ± 0.008)	15.98 (15.76 ± 0.27)	52.6 (52.1 ± 0.7)	6.64 (6.47 ± 0.17)
	3% DIO	0.764 (0.758 ± 0.007)	14.56 (14.34 ± 0.26)	46.4 (45.8 ± 0.8)	5.13 (4.95 ± 0.23)
	1% DPE	0.814 (0.808 ± 0.008)	16.33 (16.07 ± 0.30)	51.2 (52.4 ± 1.0)	6.81 (6.59 ± 0.25)
	2% DPE	0.822 (0.815 ± 0.01)	16.65 (16.39 ± 0.33)	53.5 (53.0 ± 0.9)	7.26 (7.03 ± 0.27)
	3% DPE	0.809 (0.803 ± 0.009)	15.79 (15.56 ± 0.28)	48.9 (48.3 ± 0.8)	6.25 (6.08 ± 0.20)
PDTBBT-4F:PC$_{71}$BM = 1:2	W/O	0.817 (0.812 ± 0.007)	14.25 (14.03 ± 0.24)	50.7 (50.3 ± 1.0)	5.92 (5.79 ± 0.16)
	1% DIO	0.779 (0.772 ± 0.008)	11.93 (11.70 ± 0.27)	43.8 (43.3 ± 0.9)	4.07 (3.92 ± 0.18)
	2% DIO	0.782 (0.777 ± 0.009)	12.78 (12.53 ± 0.29)	46.2 (45.7 ± 0.8)	4.61 (4.48 ± 0.19)
	3% DIO	0.743 (0.738 ± 0.007)	9.87 (9.69 ± 0.23)	42.8 (42.2 ± 0.9)	3.13 (2.98 ± 0.17)
	1% DPE	0.760 (0.752 ± 0.01)	13.02 (12.75 ± 0.32)	43.6 (43.0 ± 0.9)	4.31 (4.14 ± 0.23)
	2% DPE	0.778 (0.772 ± 0.01)	13.62 (13.38 ± 0.30)	45.6 (45.1 ± 0.9)	4.83 (4.62 ± 0.25)
	3% DPE	0.702 (0.695 ± 0.009)	10.87 (10.66 ± 0.28)	39.7 (39.2 ± 0.8)	3.02 (2.89 ± 0.20)

[a] The average values and standard deviations of 8 devices are shown in parentheses.
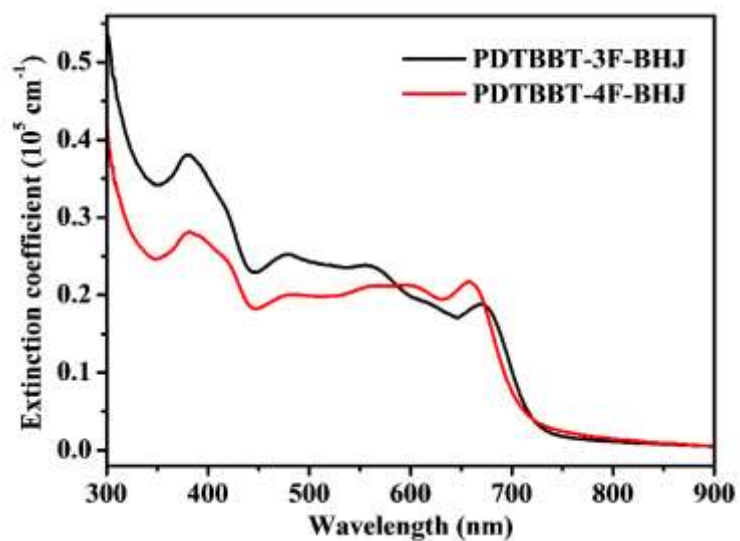
Figure S21. Extinction coefficient spectra of BHJ blend films for optimum device based on the Polymers: PC$_{71}$BM prepared from *o*-DCB.
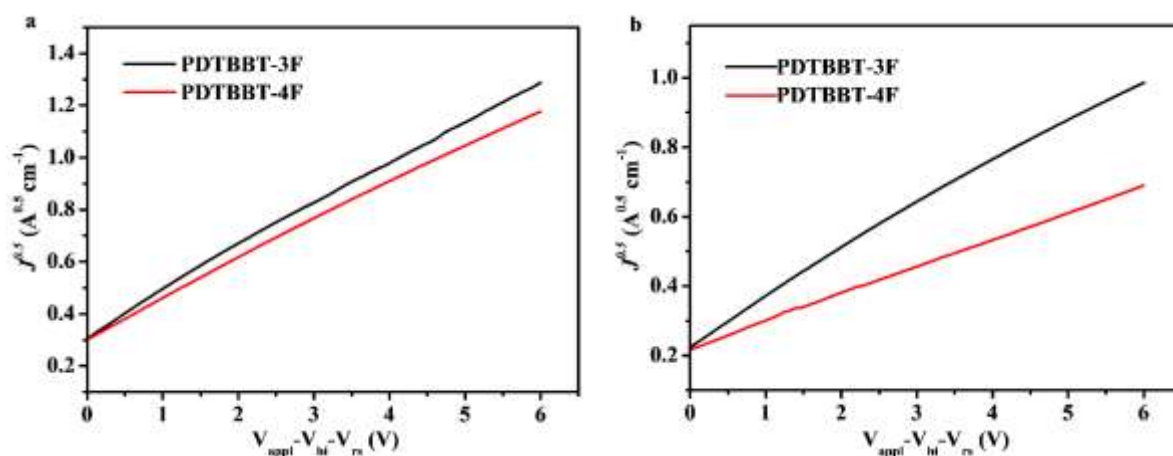

Fig. S22 $J^{0.5}$ *vs* V$_{appl}$-V$_{bi}$-V$_{rs}$ plots for a) hole-only and b) electron-only devices of **PDTBBT-3F** and **PDTBBT-4F** blend films.
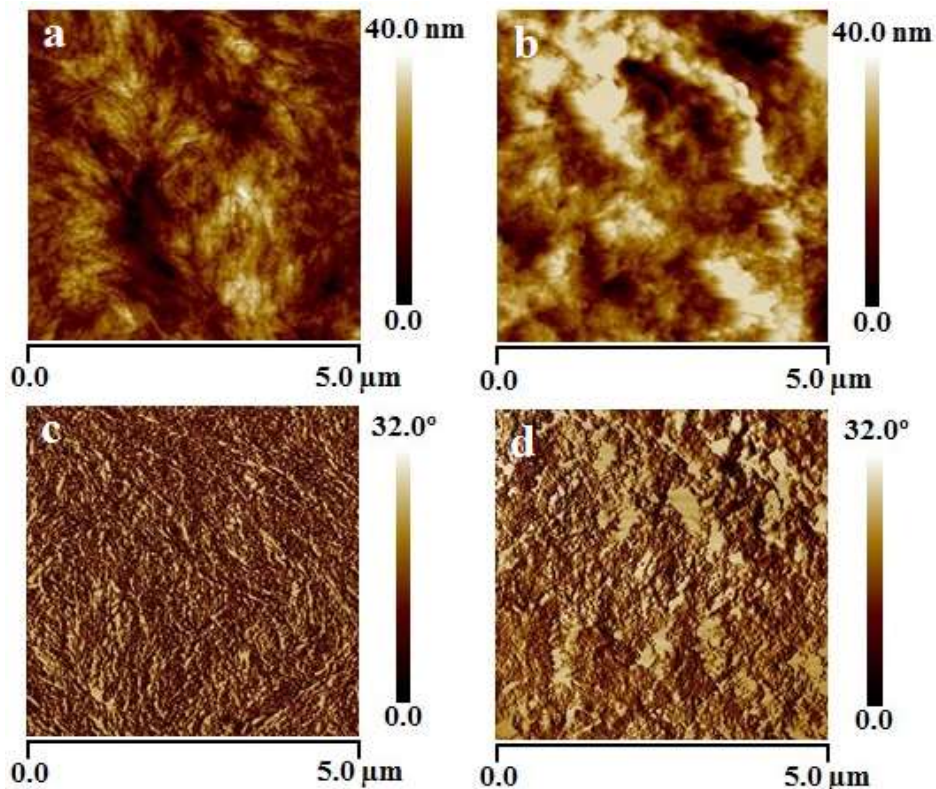
Fig. S23 Tapping-mode AFM height (a and b) and phase (c and d) images of PDTBBT-3F:PC$_{71}$BM (a and c) and PDTBBT-4F:PC$_{71}$BM (b and d) blends, respectively.

Table S3. Physical parameters of PDTBBT-3F:PC$_{71}$BM and PDTBBT-4F:PC$_{71}$BM devices.

Polymer	Leakage current at -3V (mA cm^{-2})	Rectification factor (-3V, 3V)	μ_h[a] (10^{-4} cm^2 V^{-1} s^{-1})	μ_e[a] (10^{-4} cm^2 V^{-1} s^{-1})	μ_h/μ_e
PDTBBT-3F-BHJ	0.31	680	5.65 ± 0.17	4.18 ± 0.20	1.37
PDTBBT-4F-BHJ	0.74	112	4.12 ± 0.15	0.87 ± 0.23	4.80

[a]Average values and standard deviations from 6 devices.

Table S4. The coherence length (L_C) and full width at half-maximum (FWHM) along both OOP and IP direction of the neat PDTBBT-3F and PDTBBT-4F, and the corresponding polymers:PC$_{71}$BM blend films devices (According to the Scherrer's equation, $L_C = 2\pi/fwhm$)

Polymer	OOP				IP	
	100		010		100	
	FWHM (Å^{-1})	L_C (Å)	FWHM (Å^{-1})	L_C (Å)	FWHM (Å^{-1})	L_C (Å)
PDTBBT-3F	0.0424	148.1	0.296	21.2	0.0521	120.5
PDTBBT-4F	0.0580	108.3	0.171	36.8	0.0382	164.4
PDTBBT-3F-BHJ	0.0325	193.5	0.206	30.4	0.0344	182.6
PDTBBT-4F-BHJ	0.0464	135.2	0.278	22.6	0.0512	122.6